Heliyon 9 (2023) e13194

Contents lists available at ScienceDirect

Heliyon

journal homepage: www.cell.com/heliyon

Research article

Research and development of field theory-based three-dimensional risk assessment. Part II: Regional overall risk

Fang Yan [a,*], Longjun Dong [a,**], Bing Wang [a], Tao Hu [a], Ji Ge [b]

[a] School of Resources and Safety Engineering, Central South University, Changsha, 410083, PR China
[b] School of Resources and Environmental Engineering, Jilin Institute of Chemical Technology, Jilin, 132022, PR China

ARTICLE INFO

Keywords:
Three-dimensional risk assessment
Field theory
Surface integral
Regional overall risk
Land-use planning

ABSTRACT

For three-dimensional (3D) risk assessments, the scalar fields of risk can be clarified so that the risk value at any point in 3D space can be obtained. Notably, the 3D risk function can be used to calculate the surface integral to reveal the overall risk level in a certain area. As a result, a novel field theory-based 3D risk assessment method called the regional overall risk assessment (RORA) is proposed in this study. The regional overall risk (ROR) is introduced to describe the overall risk level of the assessed area. The corresponding definition and algorithm of the ROR are determined. The selection rule of the surfaces, which are used to create the surface integrals and compute the ROR, is also provided and discussed. To demonstrate the effectiveness of the RORA, the 3D risk caused by biomass gasification stations is utilized to conduct a case study. For the assessed area (Huangtukan Village and Yanjia Village), values of ROR are 29.5787 and 39.3858, respectively. The results represent accurate overall risk levels of the assessed areas and can provide effective guidance for risk prevention in the assessed areas, including land-use planning and safety planning. Moreover, the validity and availability of the proposed RORA is verified by a sensitivity analysis. The prospects and limitations of the RORA are also analyzed and discussed in this work.

1. Introduction

1.1. Background

Three-dimensional (3D) risk assessments constitute an effective method within regional risk assessments. A scientific model of regional risk assessment can provide strong support for the risk management systems [1]. Various methods focus on the evaluations of individual risk, societal risk and risk isolines [2]. In some cases, regional risk assessments can also be called risk mapping, and has practical applications for risk assessment, risk management and risk prevention. It has been widely applied in public health, emergency management, disaster control and other fields [3–5]. Research of regional risk assessment effectively promotes the improvement of risk assessment theory. With the development of regional risk assessments, some scholars have noticed that some shortcomings exist in two-dimensional (2D) risk assessments. Among these shortcomings, the lack of height parameters may affect the assessment results. Suddle and Ale indicated that height became an important parameter for regional risk assessments because different functions are layered in 3D space [6,7]. With the addition of height to regional risk assessments, 2D risk assessments were improved and a risk

* Corresponding author.
** Corresponding author.
E-mail addresses: yanfang3543@csu.edu.cn (F. Yan), lj.dong@csu.edu.cn (L. Dong).

https://doi.org/10.1016/j.heliyon.2023.e13194
Received 25 July 2022; Received in revised form 19 January 2023; Accepted 19 January 2023
Available online 26 January 2023

isosurface can be employed to evaluate risk in 3D space. Therefore, it has important significance to research and develop 3D risk assessment.

1.2. Literature review

1.2.1. Application of 3D risk assessment

Risk is an objective quantity used to describe the degree of harm to hazards [8]. For the 3D risk assessment, the magnitude of risk value is associated with the spatial coordinates. Yet-Pole and others performed meaningful exploratory work regarding 3D risk assessments [2,9,10]. In their work, 3D risk and risk isosurfaces were calculated based on the postprocessing of computational fluid dynamics (CFD) simulations. These results contribute to enhancing the accuracy of quantitative risk assessments (QRAs). As a result, 3D risk assessments have practical applications in the fields of environmental risk assessments of mining practices, rockfall risk assessments, and risk assessments of radiation in nuclear industries [11–13]. It is necessary and significant to develop 3D risk assessments because 3D risk assessments have practical advantages for regional risk assessments. Suddle and Ale proposed a comprehensive model for 3D risk assessments that involved calculations of isosurfaces with respect to individual risks and societal risks [7]. Yet-Pole and Cheng pointed out that CFD simulation can be integrated with 3D risk assessments [2]. Then, the spatial distribution of 3D risk for a storage tank area was obtained by their proposed methodology. Lisbona et al. integrated topography and 3D CFD models to provide higher levels of confidence in predictions of the consequences of accidents [14]. Hence, the 3D risk caused by CO_2 pipelines was evaluated, and its contours were confirmed. Similarly, Scarponi et al. also took advantage of a fully 3D CFD model to assess the risk of pressure vessels exposed to fire [15]. The results showed that the risk values calculated by the 3D risk assessment were more precise than those obtained through other methods and that the 3D risk assessment will be helpful in supporting risk management strategies and emergency response planning. In the Li et al. study, an early warning model of tailings dams was established based on 3D spatial simulations and 3D risk calculations [16]. It is clear that 3D simulation-based risk analyses will provide the bases to make more reasonable engineering decisions, protection measure designs, emergency evacuations and other risk prevention measures.

1.2.2. Field theory-based 3D risk assessment

Previous research on 3D risk assessments has mainly focused on the calculation and evaluation of 3D risk itself. Moreover, 3D risk assessments have the potential to provide more detailed and deeper analyses because they can provide scalar fields of 3D risk. According to field theory analyses in physics [17], scalar fields can be converted into vector fields, and corresponding parameters, including gradient, surface integral, flux can be introduced to perform various analyses. Huang et al. proposed a system risk analysis approach called the improved risk field [8]. Risk field is a typical 3D risk assessment method. It can explain the formation process of system coupling risk in a real-world case. In our previous work, risk gradients were explored and researched based on field theory analyses [18]. A field theory-based 3D risk assessment was developed, and a novel method called the optimization of risk reduction (ORR) was proposed. The ORR can use a risk gradient to confirm the optimal risk reduction route (ORRR) based on the steepest descent method. Then, valid risk control measures can be made according to the calculation of the ORRR. Moreover, previous research has indicated that the development of field theory-based 3D risk assessments has practical application prospects for risk prevention and control. For example, risk-based design and risk maps can be utilized to conduct land-use planning for process industries [19–21]. The key of land-use planning is the evaluation of risk (such as contours of individual risk, risk rankings, calculations of overall risk, *etc*.). Regarding studies of safety capacity, it is necessary to evaluate the overall risk for the assessed target so that the actual risk level can be compared with the acceptable regional risk level [22,23]. Then, corresponding risk control measures can be implemented based on the analysis of safety capacity. Therefore, it is clear that the 3D risk surface integral can reflect the overall risk level of an assessed area according to field theory [17]. The calculation and evaluation of the overall risk in an assessed area may lead to improvements in the applications of regional risk assessments. Further research on and development of 3D risk surface integrals applied in 3D risk assessments are necessary and significant, but the existing literature lacks relevant reports.

1.3. Research goal

In summary, it is feasible to process 3D scalar fields to determine regional risk. The surface integral can be introduced to describe the overall risk level in a certain area. Risk varying with spatial coordinates can be clearly identified. Thus, the assessment results can provide more effective guidance for risk prevention and control of hazards and the areas in which hazards are located. In order to achieve this goal, a novel field theory-based 3D risk assessment method called the regional overall risk assessment (RORA) is studied in this article.

2. Methodology

2.1. Definition of field theory-based 3D risk assessment

Field theory-based 3D risk assessments are used to evaluate the hazard risks in process industries [18]. Therefore, hazardous materials and the energy released by these hazards need to be analyzed and computed first [24]. Then, the 3D risk can be assessed. Generally, accident risk is confirmed by thermal radiation, overpressure, concentrations of noxious gas, *etc*. A corresponding mathematical model can be introduced to calculate the spatial distributions of these risk components. Consequently, certain 3D risk values representing arbitrary points in a spatially assessed area can be calculated, and the spatial distribution of the 3D risk can be confirmed.

Assuming x, y, and z denote 3D coordinates, $F(x, y, z)$ is employed to describe the scalar field of 3D risk [25,26]. Meanwhile, Eq. (1) is introduced to calculate the risk isosurface, and the spatial distribution of 3D risk is visually reflected by the risk isosurface [2]:

$$F(x, y, z) = c \tag{1}$$

where c is constant.

Subsequently, the 3D risk with respect to the assessed area can be computed. Generally speaking, the 3D risk is confirmed based on its severity and probability [27–30]. As previously mentioned, 3D risk is confirmed by hazardous materials and energies, and their spatial distributions can be expressed using corresponding mathematical models. Hence, the spatial distributions of hazardous materials and energies can be converted into a severity value, and the severity can be denoted as $E(x, y, z)$. The probability of risk is confirmed based on the accident itself and is embodied as a certain value. Then the compensation factor is also employed to make calculation of 3D risk. Its value range is set as [0, 1] while its value depends on the implementation of safety measures. If the performance of safety measures is worse, the value of compensation factor will be closer to 0. On the contrary, better safety measures will result in the value closer to 1. Then, the universal algorithm of 3D risk is shown in Eq. (2).

$$F_i(x, y, z) = \varepsilon_i f_i E_i(x, y, z) \tag{2}$$

where $F_i(x, y, z)$ denotes the 3D risk, ε_i denotes the compensation factor caused by the safety measures, f_i denotes the probability of risk i, and $E_i(x, y, z)$ denotes the severity.

In general, multiple hazards may be considered in a 3D risk assessment of an assessed area. To evaluate risks caused by multiple hazards, the 3D risk can be superposed as shown in Eq. (3) below:

$$F_s(x, y, z) = \sum_{i=1}^{n} F_i(x, y, z) \tag{3}$$

where $F_s(x, y, z)$ denotes the superposed scalar field of the risk.

2.2. Regional overall risk

Assuming a scalar field $A(F)$ of risk exists in 3D space, its corresponding function is confirmed by the 3D risk $F_i(x, y, z)$ (Eq. (2)). Then, the surface integral of surface S is applied, as shown Eq. (4) [17], and the obtained value of φ is called the regional overall risk (ROR). The value of φ represents the ROR on a certain surface S. Eq. (4) can be expressed as follows:

$$\varphi = \iint_{\sum} F(x, y, z)\, dS \tag{4}$$

where φ denotes the ROR on the surface S.

In addition, the calculation of the surface integral conforms to the principle of additivity. Assuming that the scalar field function has various surfaces on which to calculate the surface integral, the superposed value of the surface integral is calculated by Eq. (5) [17]. For a field theory-based 3D risk assessment, the ROR can be evaluated by computing various surface integrals. However, the risks evaluated by various surface integrals are totally different from each other. For instance, the risk of the assessed area calculated in each certain direction must be different because external factors (such as the population density, geographical factors, building layout, etc.) of the assessed areas are different. Therefore, the weight of each surface integral needs to be considered, and Eq. (5) is modified to become Eq. (6) to facilitate the superposition of surface integrals. The resulting calculation result represents the ROR of the assessed area with respect to various surfaces. Eqs. (5) and (6) can be expressed as follows:

$$\begin{aligned} \varphi_s &= \varphi_1 + \varphi_2 + \ldots + \varphi_n \\ = \iint_{\sum = \sum_1 + \sum_2 + \ldots + \sum_n} F(x, y, z)\, dS &= \iint_{\sum_1} F(x, y, z)\, dS_1 + \iint_{\sum_2} F(x, y, z)\, dS_2 + \ldots + \iint_{\sum_n} F(x, y, z)\, dS_n \end{aligned} \tag{5}$$

where φ_s denotes the superposed value of the surface integral;

$$\varphi_s = \omega_{i_1}\varphi_{i_1} + \omega_{i_2}\varphi_{i_2} + \ldots + \omega_{i_n}\varphi_{i_n} \tag{6}$$

where ω denotes the corresponding weight of the surface integral with respect to a certain surface.

The ROR can be introduced to reflect the amount of risk within a certain area. As a result, it can be utilized to evaluate hazards, and the risks caused by hazards can be quantitatively assessed based on the calculation of the ROR. It not only takes into account risks with respect to the assessed hazards themselves but also considers the impacts of regional coordinates on the assessed risk receptors. Moreover, multiple surfaces can be constructed on which to calculate the surface integral. Then, more comprehensive and reasonable assessment results can be obtained.

2.3. Evaluation steps

The ROR can be employed to evaluate the magnitudes of risks caused by hazards in a certain area. Thus, a novel field theory-based 3D risk assessment method called the RORA is proposed. As previously mentioned, in the calculation of the ROR, 3D risk first needs to be calculated. Then, the surface should be confirmed to calculate the surface integral so that the ROR can be obtained. The key point in the ROR calculation is the selection of the surface. However, the ROR calculated by a single surface may not fully reflect the magnitudes of the risks caused by hazards. Hence, multiple surfaces need to be confirmed to make a comprehensive assessment, and the weight of each surface should also be confirmed. Finally, a 3D risk assessment of the assessed area can be made based on a comprehensive evaluation of the ROR, and this assessment can guide risk prevention and control measures for the assessed area [31]. The framework of the proposed method is provided in Fig. 1, and the main steps of the proposed RORA method are listed below.

Step 1: Risk identification of hazards in the assessed 3D area. The amount and number of hazards and the species of hazardous materials contained in the hazards need to be clarified. Then, corresponding accidents caused by hazardous materials should be confirmed. The spatial data must be confirmed with respect to hazards, risk receptors and the assessed area, including the location, size and scope of the assessed area boundary. Subsequently, a spatial rectangular coordinate system is established to prepare for the next steps.

Step 2: Calculation of the 3D risk. The 3D risks caused by hazards are calculated using Eq. (2). The compensation factor, ε, is confirmed based on the implementation of safety measures and is set as a constant. The probability of risk, f, is confirmed based on the probabilistic risk assessment (PRA) and is set as a constant. The severity, $E(x, y, z)$, is calculated according to the relevant hazardous materials and energies. To simplify this calculation, the assessed hazards are regarded as certain points in space. Consequently, a function of the 3D risk can be obtained, as shown in $F(x, y, z)$.

Step 3: Selection of surfaces. According to the mathematical and physical meaning of surface integral, value of surface integral can represent the cumulative amount of a physical variable in a certain region. 3D risk caused by hazards is reflected by several physical variables including thermal radiation, overpressure, *etc.* Notably, calculation of surface integral with respect to 3D risk $F(x, y, z)$ will indicate the overall risk in the assessed area. To evaluate the magnitudes of the risks in the assessed area, surfaces are utilized on which to calculate surface integrals so that the ROR can be obtained, thus reflecting the overall risk degree for the assessed area. In consideration of the physical characteristic of risk factor (thermal radiation, overpressure …), hemisphere surfaces and planes perpendicular to the ground are used to calculate the surface integrals (Fig. 2). The value of a surface integral with respect to a hemisphere surface can represent the overall level of risk for an assessed area. Meanwhile, the value of a surface integral with respect to a plane perpendicular to the ground indicates the magnitude of risk in a portion of the assessed area. Subsequently, the ROR of an assessed area can be computed based on the comprehensive consideration of the calculation results of the ROR with respect to the above two kinds of surfaces.

Step 4: Confirmation of the surface equation. The selected surfaces include two kinds of surfaces, *i.e.*, hemisphere surfaces and

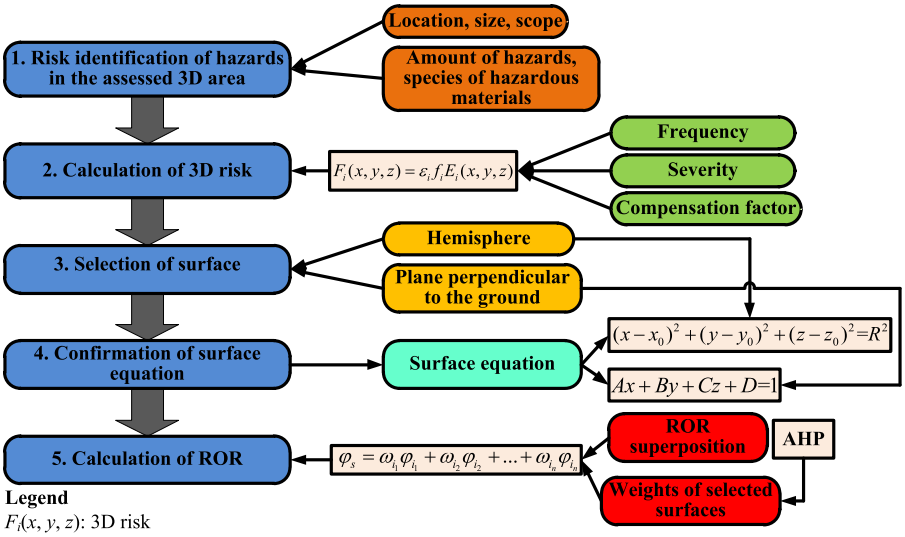

Fig. 1. Flowchart of proposed method.

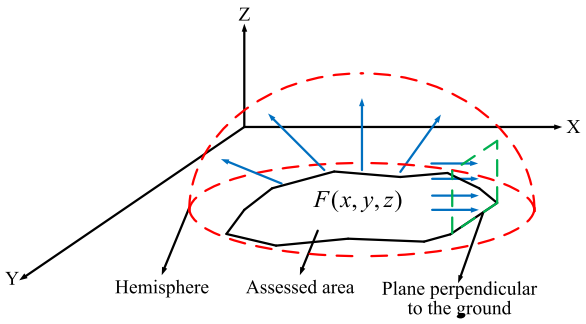

Fig. 2. Two kinds of surfaces.

planes perpendicular to the ground. The cross-section of a the hemisphere surface and horizontal plane is a circle, and the center of the circle coincides with the center of the assessed area. Hence, the hemisphere surface equation is confirmed by the radius, *i.e.*, the maximum distance from the center of the assessed area to the boundary and coordinates of the center of the assessed area. The general type of surface equation with respect to a semi-spherical surface is shown in Eq. (7). Considering that hazards may be located at the boundary of an assessed area, the value of R is set to be twice the value of the maximum distance from the center of the assessed area to the boundary. Regarding the plane perpendicular to the ground, its height is equal to the value of R, and its bottom edge coincides with a certain boundary of the assessed area. The general type of surface equation used for the plane perpendicular to the ground is shown as Eq. (8). Consequently, the corresponding surface equations are constructed based on the established spatial rectangular coordinate system. Eqs. (7) and (8) can be expressed as follows:

$$(x - x_0)^2 + (y - y_0)^2 + (z - z_0)^2 = R^2 \tag{7}$$

where R denotes the double-maximum distance from the center of the assessed area to the boundary and (x_0,y_0,z_0) denotes the coordinates of the center of the assessed area;

$$\frac{x}{A} + \frac{y}{B} + \frac{z}{C} = 1 \tag{8}$$

where A, B, and C are defined as intercepts and are confirmed based on the actual size of the plane and the spatial rectangular coordinate system.

Step 5: Calculation of the ROR. The ROR for the whole assessed area is confirmed by the superposition of each surface integral with respect to multiple surfaces. The surface integral obtained from the hemisphere surface is used to reflect the overall risk degree for the assessed area, and the surface integral obtained from the plane perpendicular to the ground is utilized to describe the magnitude of the risk in the assessed area in a certain direction. Therefore, the proposed framework in this study employs one hemisphere surface and several planes perpendicular to the ground to make evaluations. The number of planes perpendicular to the ground is determined by the evaluation requirement and actual situation. As previously mentioned, the superposition of the ROR is made by Eq. (6). The corresponding weights need to be considered. Subsequently, a pairwise comparison and a 1/9-9 scale-based analytic hierarchy process (AHP) are employed to confirm the weights of the surfaces [32]. In order to reduce the impact of uncertainty on the assessment results, no less than 10 experts in the related field from different professions should be invited to confirm the judgment matrix. For any 1/9-9 scale-based judgment value, it needs to be agreed with all invited experts, otherwise it will be rejudged. Four factors, including casualties, property damage, environmental impact and social impact, are introduced to evaluate the weight of the selected curved surface according to the conventional risk assessment method [33]. For the classification of the assessment indices used to perform analysis by the AHP, the efficacy contributing to the overall risk is set as the overall objective, the above four factors are set as middle factors, and the selected surfaces are set as criteria. The indices are established and are shown in Fig. 3. Consequently, the ROR is calculated based on the obtained weights and Eq. (6), and the overall risk degree of the assessed area can be evaluated according to the calculation results.

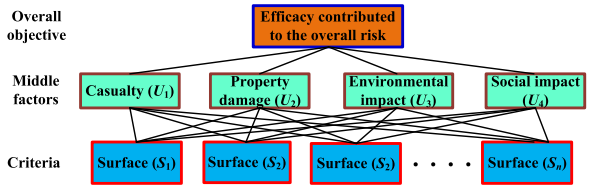

Fig. 3. Classification of assessment indices.

3. Case study

The calculation of the ROR can be used to describe the overall risk degree of an assessed area. On the other hand, the calculation of the ROR can be utilized to make system risk analysis so that risk prevention and control measures for hazards can be confirmed. To demonstrate the availability and efficiency of the ROR applied in the system risk analysis, the proposed RORA is used to conduct a 3D risk assessment of biomass gasification stations as a case study.

Biomass gas is generated through pyrolysis reactions and anoxic combustion at biomass gasification stations, and generated biomass gas is used to meet the daily needs of users [34]. Owing to the consideration of economic factors, the distance between each user and the biomass gasification station should be as short as possible. Moreover, biomass gasification stations should be built in villages to fulfill the requirement of facilitating the local collection of biomass materials. Moreover, each biomass gasification station includes one or more storage tanks, and the produced biomass gas is stored in the storage tanks before being delivered to each user. The biomass gas storage tanks contain many flammable and explosive substances, including CO, H_2, and CH_4 [34]. Therefore, fire and explosion risks caused by biomass gas storage tanks also need to be considered when confirming the locations of biomass gasification stations. In this study, the Huangtukan Village biomass gasification station and the Yanjia Village biomass gasification station (hereafter referred to as the 'Huangtukan station' and 'Yanjia station'; Figs. 4 and 5) are introduced to perform a 3D risk assessment using the RORA [34]. The two stations are located in Shenyang city, Liaoning Province, Northeast China. Huangtukan station is located at 122.767°E, 41.718°N, and Yanjia station is located at 123.750°E, 41.996°N.

Basic information regarding the above two villages is collected to support the reference conditions for the weight calculations of the selected surfaces (Table 1). Meanwhile, hazards, *i.e.*, the biomass gas storage tanks of the two assessed biomass gasification stations, are identified (Table 2). To calculate the thermal radiation and overpressure for the determination of accident consequences, the gas compositions of only flammable gases are listed in Table 2. In addition, biomass gas includes a small quantity of alkane gases, which are not listed in Table 2 because their composition composes less than 1% of the total biomass gas. Then, the corresponding rectangular coordinate system is established for the assessed area with respect to the two villages (Figs. 6 and 7).

4. Results

4.1. Calculation of 3D risk

The calculation of 3D risk needs to be made before the process of the RORA can begin. Because biomass gas has the characteristics of flammability and a low explosive limit, fire and explosion are considered accident risks in this study. As previously mentioned, 3D risk is computed by the product of the compensation factor (ε), probability (f) and severity ($E(x, y, z)$). Obviously, the confirmation of the compensation factor and probability are not affected by spatial coordinates. Moreover, the purpose of the case study is to demonstrate the proposed method, and it is unnecessary to pay attention to the accuracy of the values with respect to the compensation factor and probability [18]. To facilitate a comparison of the assessment results, the compensation factor and probability are set to the same values for both Huangtukan station and Yanjia station (Table 3).

Subsequently, the severity of the accident risk is calculated so that the 3D risk can be obtained. In consideration of the general types of fire and explosion accidents possible at the biomass gasification stations, it is assumed that the type of fire is a jet fire, and the type of explosion is a vapor cloud explosion [35]. Therefore, corresponding models can be introduced according to the available literature to calculate the thermal radiation and overpressure. Then, the accident consequences, fire and explosion, can be quantified to confirm the severity. The released gas should be confirmed before the thermal radiation is calculated (Eq. (9)) [36,37]. After confirmation, Eq. (10) is introduced to calculate the thermal radiation [38,39]. For vapor cloud explosions, selected empirical models based on experimental data are employed to compute the overpressure (Eqs. (11)–(13)) [40], as follows:

$$m_o = C_D A_h \sqrt{\gamma p \rho \left(\frac{2}{\gamma+1}\right)^{\frac{\gamma+1}{\gamma-1}}} \tag{9}$$

Fig. 4. Huangtukan station.

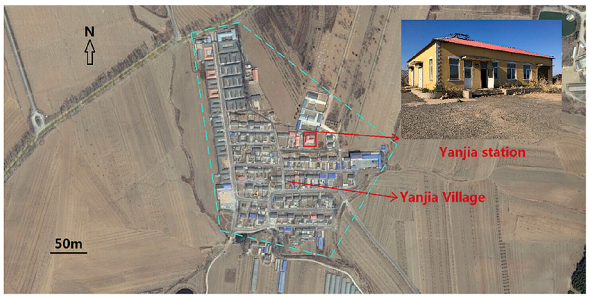

Fig. 5. Yanjia station.

Table 1
Details of Huangtukan village and Yanjia village.

Details	Huangtukan Village	Yanjia Village
North of the village	Yexing Village (approximately 1.5 km apart)	Shenyang national forest park (approximately 0.8 km apart)
South of the village	Jinjiafen Village (approximately 0.9 km apart)	Dongsijiazi Village (approximately 0.8 km apart)
East of the village	Lengzipu nine-year education school (approximately 2.2 km apart)	Huaguoshan resort (approximately 0.7 km apart)
West of the village	Liao River (approximately 1.9 km apart)	Shenyang Qipanshan international scenic tourism development zone (approximately 1.9 km apart)

Table 2
Details of hazards.

Details	Biomass gas storage tank		Biomass gas composition			Number of storage tanks
	Maximum volume (m^3)	Actual reserves (m^3)	CO	H_2	CH_4	
Huangtukan station	132	105	20.36%	10.94%	4.41%	1
Yanjia Station	393	314	22.48%	11.76%	2.10%	1

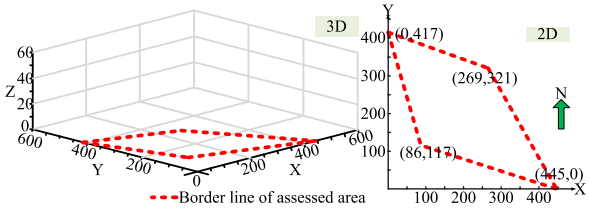

Fig. 6. Rectangular coordinate system of the assessed area (Huangtukan station).

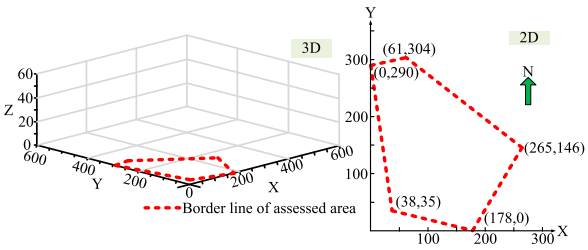

Fig. 7. Rectangular coordinate system of the assessed area (Yanjia station).

where m_o denotes the discharge rate of gas (kg/s), C_D denotes the discharge coefficient (the value of which is set to 0.61 in this study) [36,37], A_h denotes the opening area (m^2), γ denotes the ratio of specific heat capacities (C_p/C_v), p denotes the pressure of the storage tank; and ρ denotes the density (kg/m^3);

Table 3
Compensation factor and probability values.

Compensation factor (ε)	Probability (f)	
	Fire	Explosion
0.5	1×10^{-1} (in one year)	1×10^{-3} (in one year)

$$I(x,y,z) = \frac{\eta_j H_c m_o T_{jet}}{4\pi d^2} \tag{10}$$

where I (x,y,z) denotes the thermal radiation intensity (W/m^2), η_j denotes the efficiency factor, H_c denotes the heat of combustion (J/kg), T_{jet} denotes the radiation coefficient, and d denotes the distance from the assessed point to the location of the fire;

$$m_{TNT} = \frac{m_d \Delta H_d}{Q_{TNT}} \tag{11}$$

where m_{TNT} denotes the equivalent mass of TNT (kg), m_d denotes the mass of the explosive gas, ΔH_d is the heat of combustion of the explosive gas (kJ/kg), and Q_{TNT} is the heat of combustion of TNT (4601 kJ/kg);

$$Z_G = \frac{R_G}{m_{TNT}^{1/3}} \tag{12}$$

where Z_G denotes the scaled distance and R_G denotes the real distance from the assessed point to the explosion point (m); and

$$\log_{10} P_o = 0.2518(\log_{10} Z_G)^2 - 2.0225(\log_{10} Z_G) + 5.8095 \tag{13}$$

where P_o denotes the overpressure.

Consequently, the thermal radiation and overpressure caused by hazards can be confirmed based on the solutions and integrations of Eqs. (1), (9)–(13), respectively. Their calculation functions are shown as Eqs. (14) and (15) below.

$$I(x,y,z) = \frac{\eta_j H_c T_{jet} C_D A_h \sqrt{\gamma p \rho \left(\frac{2}{\gamma+1}\right)^{\frac{\gamma+1}{\gamma-1}}}}{4\pi d^2} \tag{14}$$

$$P_o(x,y,z) = 10^{0.2518\left[\log_{10}\frac{R_G Q_{TNT}^{1/3}}{(m_d \Delta H_d)^{1/3}}\right]^2 - 2.0225\left[\log_{10}\frac{R_G Q_{TNT}^{1/3}}{(m_d \Delta H_d)^{1/3}}\right] + 5.8095} \tag{15}$$

To confirm the severity value, the maximum values of thermal radiation and overpressure are introduced for normalization. In this study, individual people are considered risk receptors create the case study. Therefore, the maximum value of thermal radiation will lead to a significant chance of instantaneous fatality, and its value is set as 37.5 kW/m^2 [39]. The maximum overpressure value will lead to probable deaths of human beings, and its value is set as 50 kPa [37]. Then, the fire accident severity and explosion accident severity are calculated by Eqs. (16) and (17), respectively. Consequently, the 3D risk can be obtained based on Eqs. (2), (3), (16) and (17) and Tables 3–4 (Eqs. (18) and (19)). Eqs. (16)–(19) can be expressed as follows:

$$E_{fire}(x,y,z) = \frac{I(x,y,z)}{37.5 \times 10^3} = \frac{\eta_j H_c T_{jet} C_D A_h \sqrt{\gamma p \rho \left(\frac{2}{\gamma+1}\right)^{\frac{\gamma+1}{\gamma-1}}}}{37.5 \times 10^3 \times 4\pi d^2} \tag{16}$$

Table 4
Values of coefficients.

Coefficient	Value	
	Huangtukan station	Yanjia station
C_D	0.975	0.975
A_h	5.0×10^{-3} m^2	7.5×10^{-3} m^2
γ	1.385	1.391
p	0.525 MPa	0.713 MPa
ρ	1.107 kg/m^3	1.189 kg/m^3
η_j	0.7	0.7
H_c	1.809×10^7 J/kg	1.813×10^7 J/kg
T_{jet}	0.9	0.9
m_d	0.602×10^3 kg	2.626×10^3 kg
ΔH_d	1.809×10^7 J/kg	1.813×10^7 J/kg
Q_{TNT}	4.601×10^6 J/kg	4.601×10^6 J/kg

$$E_{\text{fire}}(x,y,z)=\frac{P_o(x,y,z)}{50\times10^3}=2\times10^{0.2518\left[\log_{10}\frac{R_G Q_{TNT}^{1/3}}{(m_d\Delta H_d)^{1/3}}\right]^2-2.0225\left[\log_{10}\frac{R_G Q_{TNT}^{1/3}}{(m_d\Delta H_d)^{1/3}}\right]+0.8095} \tag{17}$$

$$F_1(x,y,z)=\frac{3.0658}{f_1}+10^{0.2518(-1.1249+0.5\ \log_{10}f_1)^2-1.0113\ \log_{10}f_1+0.0847} \tag{18}$$

where F_1 (x,y,z) denotes the 3D risk of Huangtukan station, f_1 denotes the square of the distance from the assessed point to the hazard, and $f_1=(x\text{-}x_1)^2+(y\text{-}y_1)^2+(z\text{-}z_1)^2$, x_1, y_1, z_1 denotes the 3D coordinates of the hazard at Huangtukan station;

$$F_2(x,y,z)=\frac{5.5747}{f_2}+10^{0.2518(-1.3383+0.5\ \log_{10}f_2)^2-1.0113\ \log_{10}f_2+0.5162} \tag{19}$$

where F_2 (x,y,z) denotes the 3D risk of Yanjia station, f_2 denotes the square of the distance from the assessed point to the hazard, and $f_2 = (x–x_2)^2 + (y–y_2)^2 + (z–z_2)^2$, x_2, y_2, z_2 denotes the 3D coordinates of the hazard at Yanjia station.

4.2. Selection of surface

As the 3D risks have been obtained by Eqs. (18) and (19), the corresponding curved surfaces need to be confirmed to calculate the surface integral so that the ROR can be achieved. According to the selection rule of the surfaces as previously mentioned, the selected surfaces of the two assessed samples (Huangtukan station and Yanjia station) include hemisphere surfaces and planes perpendicular to the ground. In consideration of the boundaries and spatial distributions of the above two villages, the selected surfaces of each village include one hemisphere surface and a number of planes perpendicular to the ground. The corresponding equations of the selected surfaces are listed in Table 5, and visualizations of the selected surfaces are shown in Figs. 8 and 9.

4.3. Confirmation of weights for selected surfaces

After the surfaces have been selected and their equations have been provided, the corresponding weights of the selected surfaces need to be obtained to further calculate the ROR. Thus, 10 experts related to the field of biomass gasification are invited to make 1/9-9 scale-based pairwise comparison. Introduction of invited experts is shown in Table 6. Then a pairwise comparison and 1/9-9 scale-based AHP are utilized to calculate the weights based on the classifications of the assessment indices shown in Fig. 3. Additionally, the basic information of the two assessed villages listed in Table 1 will be used to confirm the judgment matrices as a reference. Subsequently, judgment matrices with respect to the middle factors and criteria are worked out, and the judgment matrix of the middle factors is shown as Eq. (20). Regarding Huangtukan station, the judgment matrices for its selected curved surfaces are shown as Eqs. (21)–(24). Similarly, the judgment matrices for Yanjia station's selected curved surfaces are shown as Eqs. (25)–(28).

Consequently, the weights of the selected surfaces are computed based on the AHP, and the calculation results are listed in Table 7.

4.4. Calculation of the ROR

As previously mentioned, the ground of the assessed area is considered a horizontal plane. Thus, its related z-coordinate is set as 0. According to the information of the biomass gasification stations shown in the case study, the coordinates of Huangtukan station and

Table 5
Selected surfaces.

Equation	Huangtukan Village	Yanjia Village
Hemisphere	S_{11}: $(x-220)^2+(y-203)^2+z^2=614^2$ $(0\le z\le 614)$	S_{21}: $(x-106)^2+(y-156)^2+z^2=344^2$ $(0\le z\le 344)$
Planes perpendicular to the ground	S_{12}: $\frac{x}{445}+\frac{y}{\frac{52065}{359}}=1$ $(86\le x\le 445, 0\le y\le 117, 0\le z\le 614)$	S_{22}: $\frac{x}{178}+\frac{y}{\frac{89}{2}}=1$ $(38\le x\le 178, 0\le y\le 35, 0\le z\le 344)$
	S_{13}: $\frac{x}{\frac{5977}{50}}+\frac{y}{417}=1$ $(0\le x\le 86, 117\le y\le 417, 0\le z\le 614)$	S_{23}: $\frac{x}{\frac{2204}{51}}+\frac{y}{290}=1$ $(0\le x\le 38, 35\le y\le 290, 0\le z\le 344)$
	S_{14}: $\frac{x}{\frac{37391}{32}}+\frac{y}{417}=1$ $(0\le x\le 269, 321\le y\le 417, 0\le z\le 614)$	S_{24}: $\frac{x}{-\frac{8845}{7}}+\frac{y}{290}=1$ $(0\le x\le 61, 290\le y\le 304, 0\le z\le 344)$
	S_{15}: $\frac{x}{445}+\frac{y}{\frac{142845}{176}}=1$ $(269\le x\le 445, 0\le y\le 321, 0\le z\le 614)$	S_{25}: $\frac{x}{\frac{35827}{79}}+\frac{y}{\frac{35827}{102}}=1$ $(61\le x\le 265, 146\le y\le 304, 0\le z\le 344)$
		S_{26}: $\frac{x}{178}+\frac{y}{-\frac{25988}{87}}=1$ $(178\le x\le 265, 0\le y\le 146, 0\le z\le 344)$

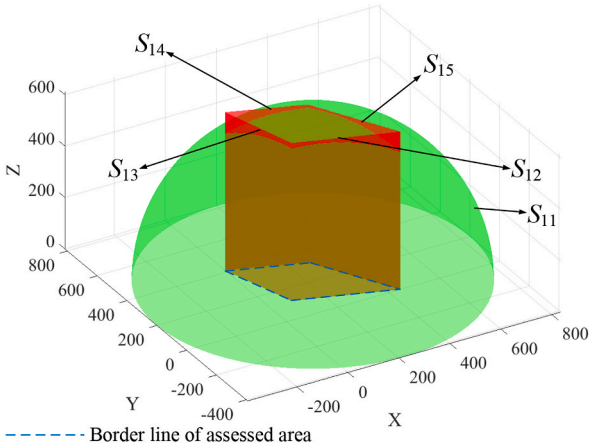

Fig. 8. Visualization of selected surfaces in the assessed area (Huangtukan station).

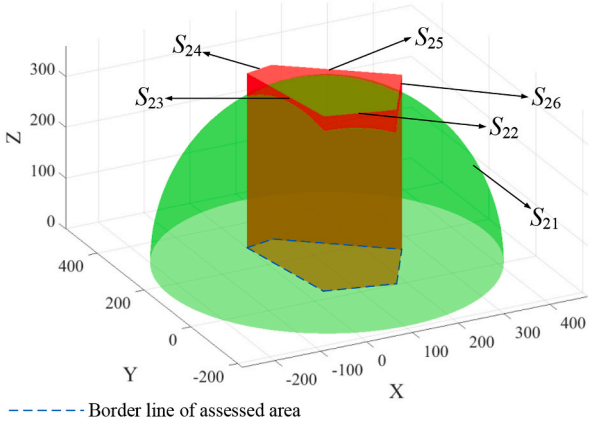

Fig. 9. Visualization of selected surfaces in the assessed area (Yanjia station).

Yanjia station are (155,184,0) and (140,187,0), respectively. Moreover, the above two stations are regarded as hazards in this study. Thus, the value of each surface integral, *i.e.*, the ROR, can be computed using MATLAB based on Eq. (4) and Table 5, and the calculation results are listed in Table 8.

As shown in Table 8, there is a significant difference between the calculation results of the ROR for the two stations. In regard to Huangtukan station, the ROR values of S_{12}~S_{15} are relatively close. This is because the location of the hazard (biomass gasification station) is close to the center of the assessed area. Moreover, the areas of the planes perpendicular to the ground (S_{12}~S_{15}) are relatively close (as shown in Fig. 8 and Table 5), which also contributes to the obtained calculation results. Because the area of S_{11} is much larger than those of S_{12}~S_{15}, its ROR value is much larger than those of S_{12}~S_{15}. For Yanjia station, the calculation results of each ROR have obvious differences. This is mainly because the location of the hazard is far from the center of the assessed area. In addition, the ROR value of S_{25} is much larger than those of the other surfaces (except S_{21}). This is caused by the following two reasons: a. S_{25} has the largest area of all planes perpendicular to the ground (as shown in Fig. 9 and Table 5); S_{25} is the surface closest to the hazard. Meanwhile, the area of S_{21} is larger than that of S_{25}, and the difference in the RORs between S_{21} and S_{25} is not as significant as the differences among the other surfaces because the larger area of S_{21} is offset by its greater distance from the hazard. Notably, the overall risk degree of assessed area in each part can be reflected by the RORs. Consequently, the RORs of the assessed areas (Huangtukan Village and Yanjia Village) are calculated based on Eq. (6), Tables 7 and 8, and the overall risk degrees for Huangtukan Village and Yanjia Village can be identified. The calculation results are listed in Table 9.

5. Discussion

5.1. Verification of the proposed method

As shown in Table 9, the overall risk degrees of Huangtukan Village and Yanjia Village in the assessed area can be confirmed. This shows that Yanjia Village has a higher risk degree than does Huangtukan Village. Notably, the volume of the actual biomass gas

Table 6
Introduction of invited experts.

$$M_U = \begin{bmatrix} \alpha_{U_1,U_1} & \alpha_{U_1,U_2} & \alpha_{U_1,U_3} & \alpha_{U_1,U_4} \\ \alpha_{U_2,U_1} & \alpha_{U_2,U_2} & \alpha_{U_2,U_3} & \alpha_{U_2,U_4} \\ \alpha_{U_3,U_1} & \alpha_{U_3,U_2} & \alpha_{U_3,U_3} & \alpha_{U_3,U_4} \\ \alpha_{U_4,U_1} & \alpha_{U_4,U_2} & \alpha_{U_4,U_3} & \alpha_{U_4,U_4} \end{bmatrix} = \begin{bmatrix} 1 & 5 & 3 & 2 \\ 1/5 & 1 & 1/2 & 1/4 \\ 1/3 & 2 & 1 & 1/2 \\ 1/2 & 4 & 2 & 1 \end{bmatrix} \tag{20}$$

$$M_{1,U_1} = \begin{bmatrix} \alpha_{S_{11},S_{11}} & \alpha_{S_{11},S_{12}} & \alpha_{S_{11},S_{13}} & \alpha_{S_{11},S_{14}} & \alpha_{S_{11},S_{15}} \\ \alpha_{S_{12},S_{11}} & \alpha_{S_{12},S_{12}} & \alpha_{S_{12},S_{13}} & \alpha_{S_{12},S_{14}} & \alpha_{S_{12},S_{15}} \\ \alpha_{S_{13},S_{11}} & \alpha_{S_{13},S_{12}} & \alpha_{S_{13},S_{13}} & \alpha_{S_{13},S_{14}} & \alpha_{S_{13},S_{15}} \\ \alpha_{S_{14},S_{11}} & \alpha_{S_{14},S_{12}} & \alpha_{S_{14},S_{13}} & \alpha_{S_{14},S_{14}} & \alpha_{S_{14},S_{15}} \\ \alpha_{S_{15},S_{11}} & \alpha_{S_{15},S_{12}} & \alpha_{S_{15},S_{13}} & \alpha_{S_{15},S_{14}} & \alpha_{S_{15},S_{15}} \end{bmatrix} = \begin{bmatrix} 1 & 2 & 6 & 4 & 3 \\ 1/2 & 1 & 4 & 2 & 1 \\ 1/6 & 1/4 & 1 & 1/3 & 1/3 \\ 1/4 & 1/2 & 3 & 1 & 1 \\ 1/3 & 1 & 3 & 1 & 1 \end{bmatrix} \tag{21}$$

$$M_{1,U_2} = \begin{bmatrix} \alpha_{S_{11},S_{11}} & \alpha_{S_{11},S_{12}} & \alpha_{S_{11},S_{13}} & \alpha_{S_{11},S_{14}} & \alpha_{S_{11},S_{15}} \\ \alpha_{S_{12},S_{11}} & \alpha_{S_{12},S_{12}} & \alpha_{S_{12},S_{13}} & \alpha_{S_{12},S_{14}} & \alpha_{S_{12},S_{15}} \\ \alpha_{S_{13},S_{11}} & \alpha_{S_{13},S_{12}} & \alpha_{S_{13},S_{13}} & \alpha_{S_{13},S_{14}} & \alpha_{S_{13},S_{15}} \\ \alpha_{S_{14},S_{11}} & \alpha_{S_{14},S_{12}} & \alpha_{S_{14},S_{13}} & \alpha_{S_{14},S_{14}} & \alpha_{S_{14},S_{15}} \\ \alpha_{S_{15},S_{11}} & \alpha_{S_{15},S_{12}} & \alpha_{S_{15},S_{13}} & \alpha_{S_{15},S_{14}} & \alpha_{S_{15},S_{15}} \end{bmatrix} = \begin{bmatrix} 1 & 3 & 7 & 4 & 4 \\ 1/3 & 1 & 3 & 2 & 2 \\ 1/7 & 1/3 & 1 & \frac{1}{4} & 1\Big/3 \\ 1/4 & 1/2 & 4 & 1 & 2 \\ 1/4 & 1/2 & 3 & 1/2 & 1 \end{bmatrix} \tag{22}$$

$$M_{1,U_3} = \begin{bmatrix} \alpha_{S_{11},S_{11}} & \alpha_{S_{11},S_{12}} & \alpha_{S_{11},S_{13}} & \alpha_{S_{11},S_{14}} & \alpha_{S_{11},S_{15}} \\ \alpha_{S_{12},S_{11}} & \alpha_{S_{12},S_{12}} & \alpha_{S_{12},S_{13}} & \alpha_{S_{12},S_{14}} & \alpha_{S_{12},S_{15}} \\ \alpha_{S_{13},S_{11}} & \alpha_{S_{13},S_{12}} & \alpha_{S_{13},S_{13}} & \alpha_{S_{13},S_{14}} & \alpha_{S_{13},S_{15}} \\ \alpha_{S_{14},S_{11}} & \alpha_{S_{14},S_{12}} & \alpha_{S_{14},S_{13}} & \alpha_{S_{14},S_{14}} & \alpha_{S_{14},S_{15}} \\ \alpha_{S_{15},S_{11}} & \alpha_{S_{15},S_{12}} & \alpha_{S_{15},S_{13}} & \alpha_{S_{15},S_{14}} & \alpha_{S_{15},S_{15}} \end{bmatrix} = \begin{bmatrix} 1 & 2 & 1/3 & 2 & 3 \\ 1/2 & 1 & 1/4 & 1 & 2 \\ 3 & 4 & 1 & 5 & 6 \\ 1/2 & 1 & 1/5 & 1 & 2 \\ 1/3 & 1/2 & 1/6 & 1/2 & 1 \end{bmatrix} \tag{23}$$

$$M_{1,U_4} = \begin{bmatrix} \alpha_{S_{11},S_{11}} & \alpha_{S_{11},S_{12}} & \alpha_{S_{11},S_{13}} & \alpha_{S_{11},S_{14}} & \alpha_{S_{11},S_{15}} \\ \alpha_{S_{12},S_{11}} & \alpha_{S_{12},S_{12}} & \alpha_{S_{12},S_{13}} & \alpha_{S_{12},S_{14}} & \alpha_{S_{12},S_{15}} \\ \alpha_{S_{13},S_{11}} & \alpha_{S_{13},S_{12}} & \alpha_{S_{13},S_{13}} & \alpha_{S_{13},S_{14}} & \alpha_{S_{13},S_{15}} \\ \alpha_{S_{14},S_{11}} & \alpha_{S_{14},S_{12}} & \alpha_{S_{14},S_{13}} & \alpha_{S_{14},S_{14}} & \alpha_{S_{14},S_{15}} \\ \alpha_{S_{15},S_{11}} & \alpha_{S_{15},S_{12}} & \alpha_{S_{15},S_{13}} & \alpha_{S_{15},S_{14}} & \alpha_{S_{15},S_{15}} \end{bmatrix} = \begin{bmatrix} 1 & 3 & 7 & 4 & 1 \\ 1/3 & 1 & 4 & 1 & 1/3 \\ 1/7 & 1/4 & 1 & 1/3 & 1/6 \\ 1/4 & 1 & 3 & 1 & 1/4 \\ 1 & 3 & 6 & 4 & 1 \end{bmatrix} \tag{24}$$

$$M_{2,U_1} = \begin{bmatrix} \alpha_{S_{21},S_{21}} & \alpha_{S_{21},S_{22}} & \alpha_{S_{21},S_{23}} & \alpha_{S_{21},S_{24}} & \alpha_{S_{21},S_{25}} & \alpha_{S_{21},S_{26}} \\ \alpha_{S_{22},S_{21}} & \alpha_{S_{22},S_{22}} & \alpha_{S_{22},S_{23}} & \alpha_{S_{22},S_{24}} & \alpha_{S_{22},S_{25}} & \alpha_{S_{22},S_{26}} \\ \alpha_{S_{23},S_{21}} & \alpha_{S_{23},S_{22}} & \alpha_{S_{23},S_{23}} & \alpha_{S_{23},S_{24}} & \alpha_{S_{23},S_{25}} & \alpha_{S_{23},S_{26}} \\ \alpha_{S_{24},S_{21}} & \alpha_{S_{24},S_{22}} & \alpha_{S_{24},S_{23}} & \alpha_{S_{24},S_{24}} & \alpha_{S_{24},S_{25}} & \alpha_{S_{24},S_{26}} \\ \alpha_{S_{25},S_{21}} & \alpha_{S_{25},S_{22}} & \alpha_{S_{25},S_{23}} & \alpha_{S_{25},S_{24}} & \alpha_{S_{25},S_{25}} & \alpha_{S_{25},S_{26}} \\ \alpha_{S_{26},S_{21}} & \alpha_{S_{26},S_{22}} & \alpha_{S_{26},S_{23}} & \alpha_{S_{26},S_{24}} & \alpha_{S_{26},S_{25}} & \alpha_{S_{26},S_{26}} \end{bmatrix} = \begin{bmatrix} 1 & 4 & 4 & 6 & 3 & 5 \\ 1/4 & 1 & 2 & 4 & 1 & 3 \\ 1/4 & 1/2 & 1 & 3 & 1/2 & 3 \\ 1/6 & 1/4 & 1/3 & 1 & 1/3 & 2 \\ 1/3 & 1 & 2 & 3 & 1 & 3 \\ 1/5 & 1/3 & 1/3 & 1/2 & 1/3 & 1 \end{bmatrix} \tag{25}$$

$$M_{2,U_2} = \begin{bmatrix} \alpha_{S_{21},S_{21}} & \alpha_{S_{21},S_{22}} & \alpha_{S_{21},S_{23}} & \alpha_{S_{21},S_{24}} & \alpha_{S_{21},S_{25}} & \alpha_{S_{21},S_{26}} \\ \alpha_{S_{22},S_{21}} & \alpha_{S_{22},S_{22}} & \alpha_{S_{22},S_{23}} & \alpha_{S_{22},S_{24}} & \alpha_{S_{22},S_{25}} & \alpha_{S_{22},S_{26}} \\ \alpha_{S_{23},S_{21}} & \alpha_{S_{23},S_{22}} & \alpha_{S_{23},S_{23}} & \alpha_{S_{23},S_{24}} & \alpha_{S_{23},S_{25}} & \alpha_{S_{23},S_{26}} \\ \alpha_{S_{24},S_{21}} & \alpha_{S_{24},S_{22}} & \alpha_{S_{24},S_{23}} & \alpha_{S_{24},S_{24}} & \alpha_{S_{24},S_{25}} & \alpha_{S_{24},S_{26}} \\ \alpha_{S_{25},S_{21}} & \alpha_{S_{25},S_{22}} & \alpha_{S_{25},S_{23}} & \alpha_{S_{25},S_{24}} & \alpha_{S_{25},S_{25}} & \alpha_{S_{25},S_{26}} \\ \alpha_{S_{26},S_{21}} & \alpha_{S_{26},S_{22}} & \alpha_{S_{26},S_{23}} & \alpha_{S_{26},S_{24}} & \alpha_{S_{26},S_{25}} & \alpha_{S_{26},S_{26}} \end{bmatrix} = \begin{bmatrix} 1 & 3 & 4 & 1/2 & 3 & 7 \\ 1/3 & 1 & 2 & 1/3 & 2 & 4 \\ 1/4 & 1/2 & 1 & 1/3 & 1 & 3 \\ 2 & 3 & 3 & 1 & 3 & 6 \\ 1/3 & 1/2 & 1 & 1/3 & 1 & 2 \\ 1/7 & 1/4 & 1/3 & 1/6 & 1/2 & 1 \end{bmatrix} \tag{26}$$

$$M_{2,U_3} = \begin{bmatrix} \alpha_{S_{21},S_{21}} & \alpha_{S_{21},S_{22}} & \alpha_{S_{21},S_{23}} & \alpha_{S_{21},S_{24}} & \alpha_{S_{21},S_{25}} & \alpha_{S_{21},S_{26}} \\ \alpha_{S_{22},S_{21}} & \alpha_{S_{22},S_{22}} & \alpha_{S_{22},S_{23}} & \alpha_{S_{22},S_{24}} & \alpha_{S_{22},S_{25}} & \alpha_{S_{22},S_{26}} \\ \alpha_{S_{23},S_{21}} & \alpha_{S_{23},S_{22}} & \alpha_{S_{23},S_{23}} & \alpha_{S_{23},S_{24}} & \alpha_{S_{23},S_{25}} & \alpha_{S_{23},S_{26}} \\ \alpha_{S_{24},S_{21}} & \alpha_{S_{24},S_{22}} & \alpha_{S_{24},S_{23}} & \alpha_{S_{24},S_{24}} & \alpha_{S_{24},S_{25}} & \alpha_{S_{24},S_{26}} \\ \alpha_{S_{25},S_{21}} & \alpha_{S_{25},S_{22}} & \alpha_{S_{25},S_{23}} & \alpha_{S_{25},S_{24}} & \alpha_{S_{25},S_{25}} & \alpha_{S_{25},S_{26}} \\ \alpha_{S_{26},S_{21}} & \alpha_{S_{26},S_{22}} & \alpha_{S_{26},S_{23}} & \alpha_{S_{26},S_{24}} & \alpha_{S_{26},S_{25}} & \alpha_{S_{26},S_{26}} \end{bmatrix} = \begin{bmatrix} 1 & 2 & 1/3 & 1/5 & 2 & 2 \\ 1/2 & 1 & 1/3 & 1/5 & 1 & 1 \\ 3 & 3 & 1 & 1/2 & 3 & 2 \\ 5 & 5 & 2 & 1 & 6 & 6 \\ 1/2 & 1 & 1/3 & 1/6 & 1 & 1 \\ 1/2 & 1 & 1/2 & 1/6 & 1 & 1 \end{bmatrix} \tag{27}$$

$$M_{2,U_4} = \begin{bmatrix} \alpha_{S_{21},S_{21}} & \alpha_{S_{21},S_{22}} & \alpha_{S_{21},S_{23}} & \alpha_{S_{21},S_{24}} & \alpha_{S_{21},S_{25}} & \alpha_{S_{21},S_{26}} \\ \alpha_{S_{22},S_{21}} & \alpha_{S_{22},S_{22}} & \alpha_{S_{22},S_{23}} & \alpha_{S_{22},S_{24}} & \alpha_{S_{22},S_{25}} & \alpha_{S_{22},S_{26}} \\ \alpha_{S_{23},S_{21}} & \alpha_{S_{23},S_{22}} & \alpha_{S_{23},S_{23}} & \alpha_{S_{23},S_{24}} & \alpha_{S_{23},S_{25}} & \alpha_{S_{23},S_{26}} \\ \alpha_{S_{24},S_{21}} & \alpha_{S_{24},S_{22}} & \alpha_{S_{24},S_{23}} & \alpha_{S_{24},S_{24}} & \alpha_{S_{24},S_{25}} & \alpha_{S_{24},S_{26}} \\ \alpha_{S_{25},S_{21}} & \alpha_{S_{25},S_{22}} & \alpha_{S_{25},S_{23}} & \alpha_{S_{25},S_{24}} & \alpha_{S_{25},S_{25}} & \alpha_{S_{25},S_{26}} \\ \alpha_{S_{26},S_{21}} & \alpha_{S_{26},S_{22}} & \alpha_{S_{26},S_{23}} & \alpha_{S_{26},S_{24}} & \alpha_{S_{26},S_{25}} & \alpha_{S_{26},S_{26}} \end{bmatrix} = \begin{bmatrix} 1 & 4 & 2 & 2 & 3 & 7 \\ 1/4 & 1 & 1/2 & 1 & 2 & 5 \\ 1/2 & 2 & 1 & 2 & 3 & 4 \\ 1/2 & 1 & 1/2 & 1 & 2 & 5 \\ 1/3 & 1/2 & 1/3 & 1/2 & 1 & 3 \\ 1/7 & 1/5 & 1/4 & 1/5 & 1/3 & 1 \end{bmatrix} \tag{28}$$

Expert	Professional position	Education background	Work experience (year)
1	Technician	Master	10
2	Technician	Bachelor	15
3	Technician	Bachelor	18
4	Engineer	PhD	9
5	Engineer	Master	14
6	Engineer	Master	21
7	Professor	PhD	16

(*continued on next page*)

Table 6 (*continued*)

Expert	Professional position	Education background	Work experience (year)
8	Professor	PhD	21
9	Professor	PhD	28
10	Professor	PhD	31

Table 7
Weights of selected surfaces.

	S_{11}	S_{12}	S_{13}	S_{14}	S_{15}	
Weight (ω)	0.3836	0.1731	0.1205	0.1245	0.1983	
	S_{21}	S_{22}	S_{23}	S_{24}	S_{25}	S_{26}
Weight (ω)	0.3507	0.1445	0.1628	0.1687	0.1232	0.0502

Table 8
Calculation results of the RORs with respect to all selected surfaces.

Huangtukan	S_{11}	S_{12}	S_{13}	S_{14}	S_{15}	
ROR	52.2155	19.4236	17.8935	11.1842	13.3029	
Yanjia	S_{21}	S_{22}	S_{23}	S_{24}	S_{25}	S_{26}
ROR	76.8921	9.7091	22.6022	4.9158	46.9306	14.4627

Table 9
Calculation results of the ROR for the assessed area.

	Huangtukan Village (φ_{s1})	Yanjia Village (φ_{s2})
ROR (φ_s)	29.5787	39.3858

reserves of the storage tank at Yanjia station is approximately triple that at Huangtukan station according to Table 2. It is easy to infer that the risk degree of Yanjia station may be higher than that of Huangtukan station. Because the other basic information differs between these two villages, the ratio of the ROR with respect to the above two stations is not completely in line with the ratio of the volume of actual reserves. However, the difference in the assessed areas of the above two villages also exerts an influence on the calculation of the ROR. Hence, a sensitivity analysis should be performed to analyze the influence of the assessed area on the calculation of the ROR. The variation ranges in the radii (of the hemisphere surfaces) and heights (of the planes perpendicular to the ground) are set as ±10%. Thus, the input values are set between 90% and 110% of the reference values. In addition, the interval of the input values is set as 1%. Then, the sensitivity analysis results are shown in Fig. 10. The sensitivity analysis results include calculations of the ROR (φ_s) and the ratio of the ROR with respect to Yanjia station and Huangtukan station ($\varphi_{s2}/\varphi_{s1}$).

As shown in Fig. 10, changes in the radii and heights of the surfaces lead to changes in the ROR values. The ROR values of Huangtukan Village and Yanjia Village increase as the radii and heights increase. In reality, the risk will be lower as the location moves farther away from the hazard. However, the ROR indicates the total risk in a certain area. Within a certain range of change, the increase of selected surfaces will lead to an increase in the ROR; that is to say, increases in the radii and heights will result in increased ROR values. In addition, the sensitivity analysis results also show the change in the ratio for the two assessed villages ($\varphi_{s2}/\varphi_{s1}$). Fig. 10 shows that the ratio $\varphi_{s2}/\varphi_{s1}$ remains almost unchanged. The variation in $\varphi_{s2}/\varphi_{s1}$ is much less than that in the ROR values (Table 10). It is reasonable that the comparison results of the two assessed villages should be stable because their actual hazard characteristics are invariable. Consequently, the overall risk degrees of the two assessed villages can be reflected by the assessment results, which are in line with their actual hazard characteristics. Hence, the validity and availability of the proposed RORA can be verified.

Moreover, expert judgment is also used to make further verification of the proposed RORA based on the established weighting criteria. As it is mentioned in Section 2.3 and Fig. 3, risk caused by the biomass gasification station can be estimated in four factors including casualty, property damage, environmental impact and social impact. Their weights can be obtained based on the judgment matrix (Eq. (20)). Weight calculation results are listed as Table 11.

Subsequently, Eq. (29) is introduced to make a brief expert judgment of the risk caused by biomass gasification station. In regard to the judgment of four factors U_1, U_2, U_3 and U_4, the standard of experts scoring is set as Fig. 11. Then 10 invited experts who have make judgment of weights of selected surfaces are re-invited to estimate the risk of assessed two biomass gasification stations. Expert judgment results are listed in Table 12. Then the total judgment score, *i.e.*, risk of assessed two biomass gasification stations is confirmed based on Eq. (29) and shown in Table 12.

$$J = \omega_{U_1}\frac{\sum_{i=1}^{N} J_{U_1,i}}{N} + \omega_{U_2}\frac{\sum_{i=1}^{N} J_{U_2,i}}{N} + \omega_{U_3}\frac{\sum_{i=1}^{N} J_{U_3,i}}{N} + \omega_{U_4}\frac{\sum_{i=1}^{N} J_{U_4,i}}{N} \tag{29}$$

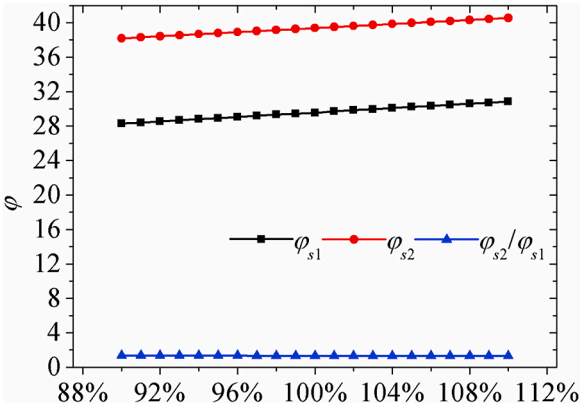

Fig. 10. Sensitivity analysis results.

Table 10
Variation in the ROR values and their ratio.

Value	φ_{s1}	φ_{s2}	$\varphi_{s2}/\varphi_{s1}$
Variation rate (from 110% to 90%)	8.3262%	5.8316%	2.6491%

Table 11
Weight calculation results of four factors.

	Casualty (U_1)	Property damage (U_2)	Environmental impact (U_3)	Social impact (U_4)
Weight (ω)	0.4773	0.0809	0.1539	0.2879

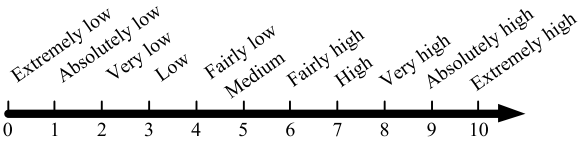

Fig. 11. The standard of experts scoring.

Table 12
Expert judgment results of Huangtukan and Yanjia biomass gasification stations.

Expert	Judgment score of risk (Huangtukan)				Judgment score of risk (Yanjia)			
	U_1	U_2	U_3	U_4	U_1	U_2	U_3	U_4
1	5	7	2	5	8	9	5	8
2	6	8	3	7	7	7	4	9
3	3	5	4	5	7	7	3	8
4	5	6	5	6	8	8	4	7
5	6	6	2	7	6	8	4	8
6	5	6	2	8	5	9	5	8
7	7	7	3	8	8	7	6	9
8	5	4	4	5	7	8	5	7
9	4	8	4	7	6	8	6	8
10	7	7	3	6	5	8	4	9
Total	5.3825				6.8770			

where J denotes the judgment score of risk, i denotes the serial number of invited expert, N denotes the total number of invited experts.

Obviously, the judgment score of risk of Yanjia biomass gasification station is higher than that of Huangtukan. It is similar to the assessment result obtained by RORA. It further verifies the validity and availability of the proposed RORA. Although traditional method (such as expert judgment mentioned in this section) can provide risk assessment result, it ignores the effect of spatial coordinates on the risk assessment. That is to say, traditional method cannot implement regional risk assessment. The influence of hazard

on the magnitude of risk in a certain assessed area cannot be considered accurately. The proposed RORA can provide quantitative 3D risk assessment, and it will make risk assessment results more accurate.

5.2. Prospects and limitations

As previously mentioned, the ROR obtained by the RORA can demonstrate the risk degrees of hazards in certain areas. Risk caused by the hazard of any coordinate in 3D space can be calculated and confirmed. As risk assessment results take into account the effect of 3D spatial coordinates, more practical risk management strategy can be made. For instance, RORA can be utilized to perform land-use planning and safety planning for an assessed area. Generally, the locations of biomass gasification stations are decided based on the most economical considerations; in other words, the distance between each user and the biomass gasification station should be as short as possible [34,41]. Nevertheless, this selection process ignores the fact that the location of biomass gasification stations will affect the overall risk degree of the assessed area. The proposed RORA approach can be introduced to solve this problem. To analyze the impacts of different locations on the overall risk degree of an assessed area, nine locations are introduced with which to calculate the RORs (Table 13).

For the information of the biomass gasification stations shown in the case study, coordinates of Huangtukan station and Yanjia station are (155,184,0) and (140,187,0). Accordingly, ROR calculation results of Huangtukan Village and Yanjia Village are 29.5787 and 39.3858, respectively (Table 9). As it can be seen in Table 9, ROR values below 29.5787 and 39.3858 are bolded and marked in red. Notably, the RORs calculated based on the actual locations of Huangtukan station and Yanjia station do not represent the minimum values. With regard to nine locations of Huangtukan station, the minimum ROR value is 29.5777, which is slightly lower than the ROR of the actual location. Moreover, two locations shown in Table 13 for Yanjia station would provide lower RORs than that of the actual location. Especially for the location (180,100,0), the corresponding ROR value is 3.9% lower than the value obtained for the actual hazard location. That is to say, actual locations of assessed biomass gasification stations are not optimal in consideration of the ROR values. Further studies can focus on methods for optimizing the locations of hazards (biomass gasification stations) considering both economic factors (such as the distance between each user and the biomass gasification station) and the ROR. Then, land-use planning and safety planning for the assessed area can be performed. And the calculation of the ROR can guide the location placements of hazards. Moreover, changes in risk management strategies within the assessed area can also be accurately quantified based on the application of RORA. For example, fire system, monitoring system and other safety measures will lead to the prevention and control of accidents caused by hazards. It will reflected in the calculation of 3D risk and ROR based on the proposed RORA. Then the risk reduction can be analyzed and evaluated quantitatively. Consequently, RORA can guide the implementation of safety measures and other risk management strategies more effective.

It is clearly that proposed RORA can provide more practical guidance for land-use planning, safety planning, safety measures and other risk management strategies. To continuously improve and develop RORA, the following limitations should be noted and studied in future work.

5.2.1. Selection of surfaces

For the proposed RORA, the selection of surfaces used to make surface integral depends on the boundary of assessed area. The bottom edge of the selected plane coincides with a certain boundary of the assessed area. In this study, the boundaries of the assessed areas were simplified as several straight lines. The actual boundaries of assessed areas will be more complex and may include combinations of straight lines and curves. Accordingly, selected surfaces should comprise planes and curved surfaces, and their equations need to be confirmed correspondingly. These adjustments will contribute to more accurate assessment results. This will dramatically increase the amount of computation. Therefore, development of calculation code will make contribution to enhance the computing efficiency.

5.2.2. Confirmation of weights for selected surfaces

An AHP was employed to confirm the surface weights in this study, which is relatively subjective. Whereas this paper intends to represent a novel 3D risk assessment method, its core idea is the establishment of a novel algorithm based on the surface integral. In order to better demonstrate the proposed method, AHP is utilized to confirm the weight due to it is relatively simple to implement. However, each selected surface must have different impact on the calculation of ROR according to the mathematical and physical

Table 13
ROR values of Huangtukan Village and Yanjia Village with different biomass gasification station locations.

Location coordinate of the hazard	Huangtukan Village (φ_{s1})	Location coordinate of the hazard	Yanjia Village (φ_{s2})
(100,150,0)	31.0568	(60,50,0)	44.1780
(220,120,0)	29.4301	(170,20,0)	41.6731
(380,60,0)	34.1841	(250,140,0)	41.4344
(100,240,0)	**29.5777**	(40,270,0)	44.2305
(220,220,0)	29.7463	**(100,100,0)**	**39.1002**
(330,150,0)	32.8290	**(180,100,0)**	**37.8491**
(40,380,0)	31.2035	(60,230,0)	41.5023
(160,330,0)	30.2887	(140,210,0)	40.8961
(250,310,0)	32.0990	(120,250,0)	45.7232

meaning of surface integral. Hence the weight of each selected surface needs to be confirmed. Generally speaking, confirmation of index weight mainly depends on expert based decision making. It leads to the results suffer from randomness and fuzziness of uncertainty. In future work, other methods, including cloud model (CM), set pair analysis (SPA), fuzzy methods, *etc*., can be employed to reduce the impact of subjectivity and promote the effectiveness of RORA. Furthermore, data collected from field investigation including hydrology data, geology data, etc., can be referred to enhance the objectivity of weight confirmation.

5.2.3. Utilization of risk flux

Risk is an objective quantity applied to describe the degree of harm to a specific hazard. The proposed RORA focuses on the evaluation of the overall risk degree for an assessed area. Considering the flux is obtained by the calculation of integral. It is similar to the calculation of ROR. Therefore, a risk gradient could be employed to make surfaces integral so that the risk flux can be obtained. The risk flux indicates that the risk source can diverge risk flux to the outside space, and the direction of risk flux is from the risk source to the external space [8]. Then, risk flux can be introduced to describe the dynamic change of 3D risk in a certain area. It has potential to make further development of RORA by combining with the risk flux.

6. Conclusion

In this study, a novel method called the RORA was proposed to evaluate the overall risk level in a certain area. 3D risk assessment results of two biomass gasification stations and their located villages show that the overall risk levels of the assessed areas can be accurately derived. In conclusion, according to the verification of validity and availability of the proposed RORA, accurate risk assessment results for a certain area can be obtained by RORA. The variation of risk with spatial coordinates can be identified and analyzed. In addition, the RORA can effectively guide the land-use planning, safety planning and other risk management strategies for assessed areas. It provides an important theoretical basis for the development of 3D risk assessment.

Author contribution statement

Fang Yan: Conceived and designed the experiments; Performed the experiments; Analyzed and interpreted the data; Contributed reagents, materials, analysis tools or data; Wrote the paper.

Longjun Dong: Conceived and designed the experiments; Contributed reagents, materials, analysis tools or data; Wrote the paper.

Bing Wang: Performed the experiments; Analyzed and interpreted the data; Contributed reagents, materials, analysis tools or data.

Tao Hu: Performed the experiments; Analyzed and interpreted the data.

Ji Ge: Contributed reagents, materials, analysis tools or data.

Funding statement

Prof. Fang Yan was supported by National Natural Science Foundation of China [52104108]; Natural Science Foundation of Hunan Province [2021JJ40767].

Bing Wang was supported by Natural Science Foundation of Hunan Province [2021JJ40799].

Data availability statement

The authors do not have permission to share data.

Declaration of interest's statement

The authors declare no conflict of interest.

References

[1] H.M. Guo, L.H. Cheng, S.G. Li, H.F. Lin, Regional risk assessment methods in relation to urban public safety, Process Saf. Environ. Protect. 143 (2020) 361–366, https://doi.org/10.1016/j.psep.2020.07.012.

[2] I. Yet-Pole, T.L. Cheng, The development of a 3D risk analysis method, J. Hazard Mater. 153 (1–2) (2008) 600–608, https://doi.org/10.1016/j.jhazmat.2007.09.003.

[3] I.C. Chen, S. Ng, G.S. Wang, H.W. Ma, Application of receptor-specific risk distribution in the arsenic contaminated land management, J. Hazard Mater. 262 (2013) 1080–1090, https://doi.org/10.1016/j.jhazmat.2012.07.045.

[4] M. Zhao, X. Liu, Regional risk assessment for urban major hazards based on GIS geoprocessing to improve public safety, Saf. Sci. 87 (2016) 18–24, https://doi.org/10.1016/j.ssci.2016.03.016.

[5] T. Le, C. Sun, S. Choy, Y. Kuleshov, Regional drought risk assessment in the central highlands and the South of Vietnam, Geomatics, Nat. Hazards Risk 12 (1) (2021) 3140–3159, https://doi.org/10.1080/19475705.2021.1998232.

[6] S. Suddle, Three-dimensional individual and group risk approach of buildings above roads and railways during exploitation. Berlin, Germany, in: Joint Meeting of the 7th International Conference on Probabilistic Safety Assessment and Management/European Safety and Reliability Conference, 2004.

[7] S. Suddle, B. Ale, The third spatial dimension risk approach for individual risk and group risk in multiple use of space, J. Hazard. Mater. 123 (1–3) (2005) 35–53, https://doi.org/10.1016/j.jhazmat.2005.04.024.

[8] W.C. Huang, B. Shuai, R. Zhang, M.H. Xu, Y.F. Xu, Y.C. Yu, E. Antwi, A new system risk definition and system risk analysis approach based on improved risk field, IEEE Trans. Reliab. 69 (4) (2020) 1437–1452, https://doi.org/10.1109/TR.2019.2942373.

[9] I. Yet-Pole, C.H. Lee, T.L. Cheng, Development and applications of CPR-A 3D consequence analysis software for educational use, J. Loss Prevent. Proc. 20 (3) (2007) 251–259.

[10] I. Yet-Pole, C.M. Shu, C.H. Chong, Applications of 3D QRA technique to the fire/explosion simulation and hazard mitigation within a naphtha-cracking plant, J. Loss Prevent. Proc. 22 (4) (2009) 506–515, https://doi.org/10.1016/j.jlp.2009.04.002.

[11] P. Wycisk, T. Hubert, W. Gossel, C. Neumann, High-resolution 3D spatial modelling of complex geological structures for an environmental risk assessment of abundant mining and industrial megasites, Comput. Geosci. 35 (1) (2009) 165–182, https://doi.org/10.1016/j.cageo.2007.09.001.

[12] F. Agliardi, G.B. Crosta, P. Frattini, Integrating rockfall risk assessment and countermeasure design by 3D modelling techniques, Nat. Hazards Earth Syst. Sci. 9 (4) (2009) 1059–1073, https://doi.org/10.5194/nhess-9-1059-2009.

[13] I. Szoke, M.N. Louka, T.R. Bryntesen, J. Bratteli, S.T. Edvardsen, K.K. RoEitrheim, K. Bodor, Real-time 3D radiation risk assessment supporting simulation of work in nuclear environments, J. Radiol. Prot. 34 (2) (2014) 389–416, https://doi.org/10.1088/0952-4746/34/2/389.

[14] D. Lisbona, A. McGillivray, J.L. Saw, S. Gant, M. Bilio, M. Wardman, Risk assessment methodology for high-pressure CO_2 pipelines incorporating topography, Process Saf. Environ. Protect. 92 (1) (2014) 27–35, https://doi.org/10.1016/j.psep.2013.09.003.

[15] G.E. Scarponi, G. Landucci, A.M. Birk, V. Cozzani, An innovative three-dimensional approach for the simulation of pressure vessels exposed to fire, J. Loss Prevent. Proc. 61 (2019) 160–173, https://doi.org/10.1016/j.jlp.2019.06.008.

[16] S.M. Li, L.W. Yuan, H. Yang, H.M. An, G.J. Wang, Tailings dam safety monitoring and early warning based on spatial evolution process of mud-sand flow, Saf. Sci. 124 (2020) 1–9, https://doi.org/10.1016/j.ssci.2019.104579.

[17] H.M. Schey, Div, Grad, Curl, and All that: an Informal Text on Vector Calculus, W. W. Norton & Company, New York, 2005.

[18] F. Yan, C. Jin, Z.J. Li, R.H. Cao, K.L. Xu, Research and development of field theory-based 3D risk assessment. Part I: optimization of risk reduction, Saf. Sci. 120 (2019) 312–322, https://doi.org/10.1016/j.ssci.2019.07.018.

[19] C. Basta, J.M.M. Neuvel, S. Zlatanova, B. Ale, Risk-maps informing land-use planning processes – a survey on The Netherlands and the United Kingdom recent developments, J. Hazard. Mater. 145 (1–2) (2007) 241–249, https://doi.org/10.1016/j.jhazmat.2006.11.032.

[20] N.H.W. van Xanten, C.M. Pietersen, H.J. Pasman, P. van der Torn, H.K. Vrijling, A.J. van der Wal, J.G.M. Kerstens, Risk evaluation in Dutch land-use planning, Process Saf. Environ. 92 (4) (2014) 368–376, https://doi.org/10.1016/j.psep.2014.06.002.

[21] N. Khakzad, G. Reniers, Risk-based design of process plants with regard to domino effects and land use planning, J. Hazard Mater. 299 (2015) 289–297, https://doi.org/10.1016/j.jhazmat.2015.06.020.

[22] G.H. Chen, S.K. Wang, X.Q. Tan, Evaluation model for safety capacity of chemical industrial park based on acceptable regional risk, Chin. J. Chem. Eng. 23 (1) (2015) 121–127, https://doi.org/10.1016/j.cjche.2014.09.039.

[23] R. Wang, M.G. Zhang, Y.T. Chen, C.J. Qian, Study on safety capacity of chemical industrial park in operation stage. Beijing, PRC, in: 9th International Symposium on Safety Science and Technology (ISSST), 2015.

[24] J. Ge, Y.Y. Zhang, K.L. Xu, J.S. Li, X.W. Yao, C.Y. Wu, S.Y. Li, F. Yan, J.J. Zhang, Q.W. Xu, A new accident causation theory based on systems thinking and its systemic accident analysis method of work systems, Process Saf. Environ. Protect. 158 (2022), https://doi.org/10.1016/j.psep.2021.12.036.

[25] S. Weinberg, Effective field theory for inflation, Phys. Rev. D 77 (12) (2008), https://doi.org/10.1103/PhysRevD.77.123541.

[26] F. Yan, L.J. Dong, B. Wang, J. Ge, B. Wang, Using risk meshing to improve three-dimensional risk assessment of chemical industry, Process Saf. Environ. Protect. 168 (2022) 1166–1178, https://doi.org/10.1016/j.psep.2022.10.078.

[27] F. Yan, K.L. Xu, A set pair analysis based layer of protection analysis and its application in quantitative risk assessment, J. Loss Prevent. Proc. 55 (2018) 313–319, https://doi.org/10.1016/j.jlp.2018.07.007.

[28] Q.W. Xu, K.L. Xu, Mine safety assessment using gray relational analysis and bow tie model, PLoS One 13 (3) (2018), https://doi.org/10.1371/journal.pone.0193576.

[29] L. Chen, Y.C. Huang, R.Z. Bai, A. Chen, Regional disaster risk evaluation of China based on the universal risk model, Nat. Hazards 89 (2) (2017) 647–660, https://doi.org/10.1007/s11069-017-2984-2.

[30] E. Ilbahar, A. Karasan, S. Cebi, C. Kahraman, A novel approach to risk assessment for occupational health and safety using Pythagorean fuzzy AHP & fuzzy inference system, Saf. Sci. 103 (2018) 124–136, https://doi.org/10.1016/j.ssci.2017.10.025.

[31] L.J. Dong, Z. Tang, X.B. Li, Y.C. Chen, J.C. Xue, Discrimination of mining microseismic events and blasts using convolutional neural networks and original waveform, J. Cent. South Univ. 27 (10) (2020) 3078–3089, https://doi.org/10.1007/s11771-020-4530-8.

[32] T.L. Saaty, J.M. Alexander, Conflict Resolution: the Analytic Hierarchy Process, Praeger Publishers, New York, 1989.

[33] T. Deacon, P.R. Amyotte, F.I. Khan, Human error risk analysis in offshore emergencies, Saf. Sci. 48 (6) (2010) 803e818, https://doi.org/10.1016/j.ssci.2010.02.013.

[34] F. Yan, K.L. Xu, D.S. Li, X.M. Zhang, Hazard assessment for biomass gasification station using general set pair analysis, Bioresources 11 (4) (2016) 8307–8324, https://doi.org/10.15376/biores.11.4.8307-8324.

[35] K.R. Cummer, R.C. Brown, Ancillary equipment for biomass gasification, Biomass Bioenergy 23 (2002) 113–128, https://doi.org/10.1016/S0961-9534(02)00038-7.

[36] J.L. Woodward, Estimating the Flammable Mass of a Vapor Cloud, CCPS AiChE, US, 1999.

[37] A.M. Shariff, R. Rusli, C.T. Leong, V.R. Radhakrishnan, A. Buang, Inherent safety tool for explosion consequences study, J. Loss Prevent. Proc. 19 (5) (2006) 409–418, https://doi.org/10.1016/j.jlp.2005.10.008.

[38] W. Carter, Condensed atmospheric photooxidation mechanisms for isoprene, Atmos. Environ. 30 (1996) 4275–4290.

[39] S.M. Tauseef, R. Suganya, T. Abbasi, S.A. Abbasi, Chemical accident simulation tool (CAST): a system for assessing consequences of accidents in chemical process industry, J. Fail. Anal. Prev. 18 (1) (2018) 101–116, https://doi.org/10.1007/s11668-018-0386-8.

[40] S. Dan, D.J. Moon, E.S. Yoon, D. Shin, Analysis of gas explosion consequence models for the explosion risk control in the new gas energy filling stations, Ind. Eng. Chem. Res. 52 (22) (2013) 7265–7273, https://doi.org/10.1021/ie302511d.

[41] F. Yan, K.L. Xu, Application of a cloud model-set pair analysis in hazard assessment for biomass gasification stations, PLoS One 12 (1) (2017) 1–17, https://doi.org/10.1371/journal.pone.0170012.